JOURNAL OF GEOPHYSICAL RESEARCH: SOLID EARTH, VOL. 118, 709–723, doi:10.1029/2012JB009473, 2013

Active tectonics of northwestern U.S. inferred from GPS-derived surface velocities

Robert McCaffrey,[1] Robert W. King,[2] Suzette J. Payne,[3] and Matthew Lancaster[1]

Received 21 May 2012; revised 25 October 2012; accepted 29 October 2012; published 14 February 2013.

[1] Surface velocities derived from GPS observations from 1993 to 2011 at several hundred sites across the deforming northwestern United States are used to further elucidate the region's active tectonics. The new velocities reveal that the clockwise rotations, relative to North America, seen in Oregon and western Washington from earlier GPS observations, continue to the east to include the Snake River Plain of Idaho and south into the Basin and Range of northern Nevada. Regional-scale rotation is attributed to gravitationally driven extension in the Basin and Range and Pacific-North America shear transferred through the Walker Lane belt aided by potentially strong pinning below the Idaho Batholith. The large rotating section comprising eastern Oregon displays very low internal deformation rates despite seismological evidence for a thin crust, warm mantle, organized mantle flow, and elevated topography. The observed disparity between mantle and surface kinematics suggests that either little stress acts between them (low basal shear) or that the crust is strong relative to the mantle. The rotation of the Oregon block impinges on Washington across the Yakima fold-thrust belt where shortening occurs in a closing-fan style. Elastic fault locking at the Cascadia subduction zone is reevaluated using the GPS velocities and recently published uplift rates. The 18 year GPS and 80 year leveling data can both be matched with a common locking model suggesting that the locking has been stable over many decades. The rate of strain accumulation is consistent with hundreds of years between great subduction events.

Citation: McCaffrey, R., R. W. King, S. J. Payne, and M. Lancaster (2013), Active tectonics of northwestern U.S. inferred from GPS-derived surface velocities, *J. Geophys. Res. Solid Earth*, *118*, 709–723, doi:10.1029/2012JB009473.

1. Introduction

[2] The plate-boundary tectonics of the western U.S. can be described very generally as the shear interaction between the Pacific and North American plates south of the Mendocino Triple Junction (MTJ) and convergence between North America and the Juan de Fuca plate north of the MTJ (Figure 1) [*Atwater*, 1970]. South of the MTJ the deformation of the North American continent occurs largely by strike-slip faulting, the San Andreas being the dominant fault, while to the north of the MTJ subduction and rotations of large blocks of continental crust appear to accommodate relative motions. The difference in tectonic style in the two regions may be related in a broad sense to the change from a shear boundary to subduction [*Humphreys and Coblentz*, 2007]. While north of the MTJ the plate boundary is largely offshore, subduction and crustal deformation that occurs onshore has potential hazards for populated regions in the U.S. Pacific Northwest [e.g., *Atwater* ,1987; *Nelson et al*., 2003].

[3] In this paper, we extend the analysis of *McCaffrey et al*. [2007] (hereafter referred to as MC07) by using an additional 6 years of GPS observations and extending the velocity field to east of Yellowstone and southward into Northern California and Nevada (Figure 2). These new data reveal that the clockwise rotations seen earlier in the GPS velocities extend far outside Oregon and Washington east to the Snake River Plain and the Wasatch Front and south into Nevada. Hence, the causes of the rotation may have much broader geodynamic implications than local block tectonics. In addition the new velocities are used to examine the kinematics of the Pacific Northwest (PNW) deformation and, along with recently published uplift rates of *Burgette et al*. [2009], to examine the interseismic locking pattern on the Cascadia subduction zone.

2. Data and Methods

2.1. Analysis

[4] The GPS velocity field (Figure 2) is updated from our 2005 field (presented in MC07) by the addition of many new continuous (cGPS) sites, extended observation times at many more, and new survey-mode (sGPS) observations in 2008, 2009, 2010, and 2011. The new sGPS observations were made largely in eastern Oregon and southern Idaho, focusing

All Supporting Information may be found in the online version of this article.

[1]Department of Geology, Portland State University, Portland, Oregon, USA.
[2]Department of Earth, Atmospheric and Planetary Sciences, Massachusetts Institute of Technology, Cambridge, Massachusetts, USA.
[3]Idaho National Laboratory, Idaho Falls, Idaho, USA.

Corresponding author: R. McCaffrey, Department of Geology, Portland State University, PO Box 751, Portland, OR 97207 USA. (mccafr@gmail.com)

2169-9313/13/2012JB009473

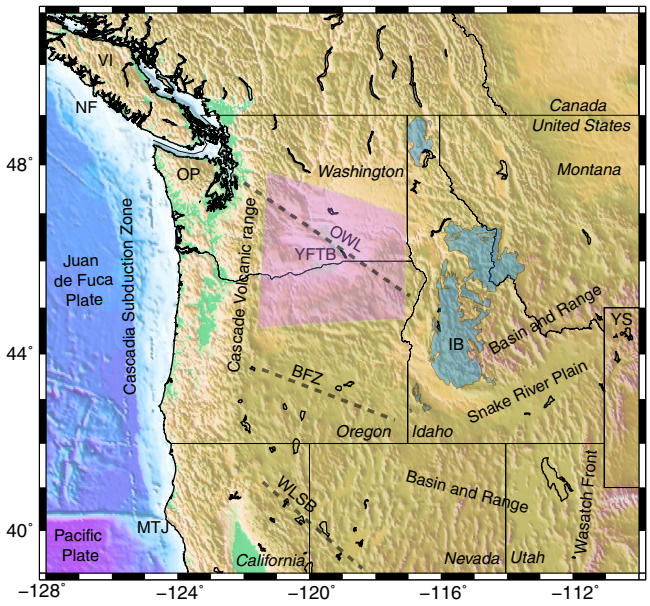

Figure 1. Physiographic map of the U.S. Pacific Northwest. Gray dashed lines show the Brothers Fault zone (BFZ), Olympic-Wallowa Lineament (OWL) and Walker Lane Shear Belt (WLSB). MTJ – Mendocino Triple Junction, YS – Yellowstone, OP – Olympic Peninsula, VI – Vancouver Island, NF – Nootka fault. Shaded regions are the Yakima fold-thrust belt (YFTB) and Idaho Batholith (IB).

on the relationship of the Snake River Plain to adjacent Basin and Range extension and rotation of Oregon [*Payne et al.*, 2008, 2012]. In 2011 we occupied 40 sGPS sites between the coast and Portland OR and east of Portland along the Columbia River. Many sGPS points from U.S. Geological Survey (http://earthquake.usgs.gov/monitoring/gps/) profiles and surveys [e.g., *Svarc et al.*, 2002] were included in the processing. The velocity field was also expanded by inclusion of processed cGPS network data obtained from the Scripps Orbit and Permanent Array Center (http://sopac.ucsd.edu) daily solutions for 1994 to 2011, Basin and Range Geodetic Network [*Wernicke et al.*, 2000], Yellowstone - Snake River Plain GPS Network (http://www.uusatrg.utah.edu/ts_ysrp.html), Pacific Northwest Geodetic Array [*Khazaradze et al.*, 1999; *Miller et al.*, 1998], National Geodetic Survey Continuously Operating Reference Sites (http://www.ngs.noaa.gov), Plate Boundary Observatory (http://www.earthscope.org/observatories/pbo), Western Canada Deformation Array [*Dragert and Hyndman*, 1995], Bay Area Regional Deformation Array (http://www.ncedc.org/bard/), and Idaho National Laboratory Snake River Plain network. In all, the number of horizontal GPS velocities meeting our criteria for tectonic interpretations increased from ~400 in the 2005 field to over 600 in this one and the sum of the weights ($\sum\sigma^{-2}$) increased by a factor of ~4.

[5] We analyze the GPS data using the GAMIT/GLOBK software [*Herring et al.*, 2010] following the approach described in section 2.2 of MC07. The velocities are determined relative to the Stable North American Reference Frame [*Herring et al.*, 2008] by estimating a six-parameter transformation (three translation rates and three rotation rates) while minimizing the adjustments from the Plate Boundary Observatory velocity field of 169 continuous stations in North America. Vertical rates of motion are estimated at all sites but for the deformation modeling we use only those within about 50 km of the coast that display linearity and consistency. As we discuss in more detail in section 3.5, we do not apply corrections to the velocity field as others have done [e.g., *Puskas and Smith*, 2009; *Pollitz et al.*, 2010] to account for postseismic mantle relaxation from past earthquakes.

2.2. Uncertainties

[6] Our error model incorporates both random and correlated noise calibrated to obtain velocity uncertainties consistent with the confidence levels of their error ellipses, as described by MC07. Our assessment of the uncertainties in horizontal velocity estimates is based on an error model for

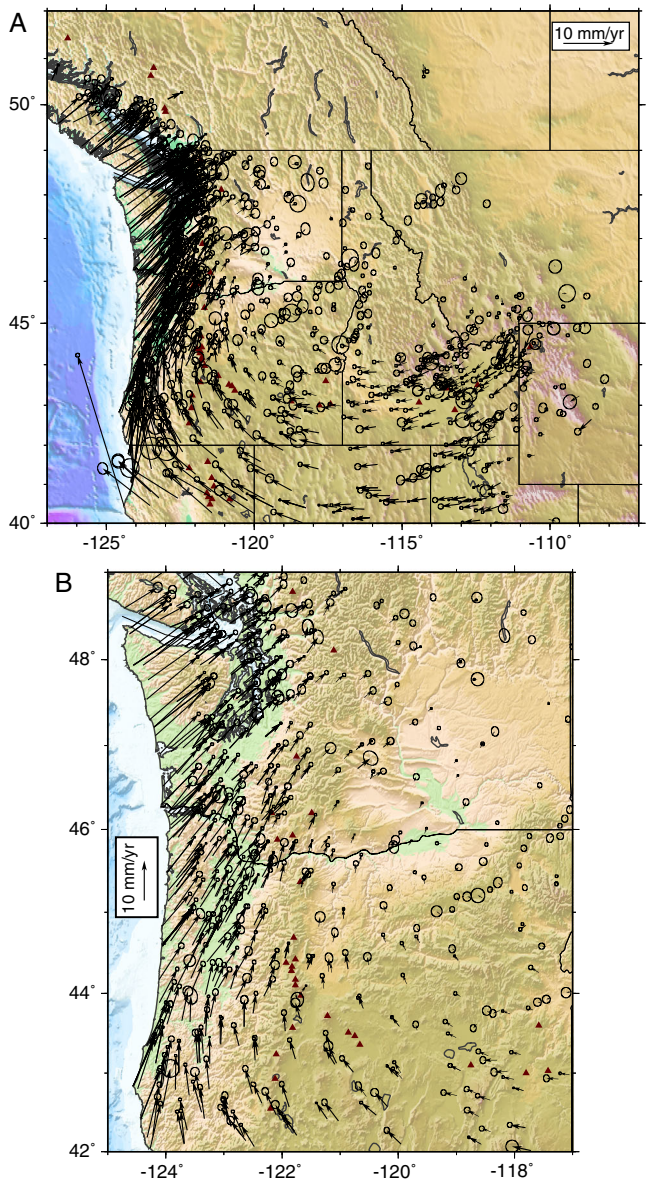

Figure 2. (a) The 1993–2011 GPS velocity field of the western U.S. relative to North America. Error ellipses are 70% confidence. Triangles denote volcanoes [*Siebert and Simkin*, 2002]. (b) Close-up of the Cascadia margin.

GPS measurements calibrated by examining residuals in a region of low strain rates. The white noise contribution to the error model is typically 0.5–1.5 mm, derived from the long-period scatter from observation sessions of 15 or more hours. Numerous studies of the spectra of continuous GPS time series have shown that the correlated component of the noise can typically be represented by a power-law with exponent –0.5 to –1.5 ("fractal white noise" or, if an exponent of –1, "flicker noise") [e.g., *Williams*, 2003]. This error model cannot be applied directly in our Kalman filter estimator, so we use the algorithm described in *Herring* [2004], *Reilinger et al.* [2006], and *Shen et al.* [2011], which fits the RMS scatter from averaging over a range of time intervals to an exponential function representing a first-order Gauss-Markov process. When evaluated for infinite averaging time, the function gives the value for the random-walk that will produce a velocity uncertainty consistent with the time-series behavior (for more details, see the "Error Analysis" presentation at http:www-gpsg.mit.edu/~simon/gtgk/Lima11/Index.html). Applying this algorithm to time series for continuous stations in the PNW yields a median value for the random-walk component of ~0.5 mm/sqrt(yr). To validate our error model we examine the velocity field for eastern Oregon and western Idaho (Figure 3). In Figure 3 we show the residual velocities, after rotating into a local reference frame and estimating a uniform horizontal strain tensor (three parameters), for the 90 sites that have velocity uncertainties less than 0.8 mm/yr. The normalized RMS (nrms) of the GPS residuals is 1.08 (1.11 for east component and 1.04 for the north) and the weighted RMS is 0.38 mm/yr in both the north and east. Our scheme of assigning uncertainties results in good agreement with a Gaussian distribution for both east and north components (Figure 3b).

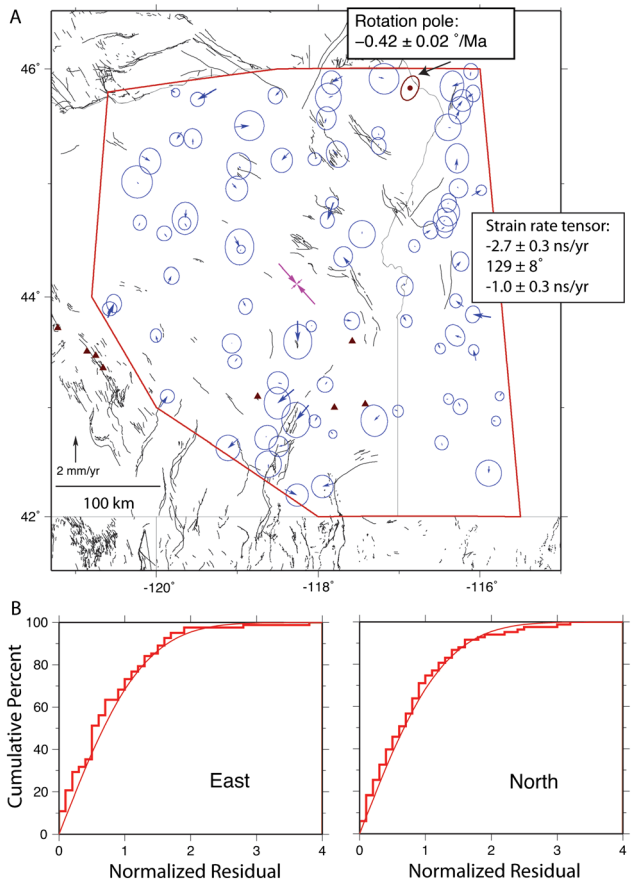

Figure 3. (a) Residual velocities after removing horizontal uniform strain rates in an eastern Oregon reference frame. Ellipses are at 70% confidence. Opposing purple arrows show principal strain rates estimated from the velocities. (b) Distribution of normalized residuals (histogram) compared to theoretical curve for Gaussian distribution (smooth curve).

2.3. 2011 GPS Velocity Field

[7] The resulting velocity field encompasses most of the active plate boundary north of 40°N (Figure 2a) with the exception of the Mendocino Triple Junction (MTJ) area (velocities are listed in the auxiliary material).[1] Large spatial gaps exist in the regions of the Idaho Batholith and western Montana where rugged terrain hinders access. We have installed and occupied some marks in these regions that will eventually yield useful velocity estimates.

[8] The first-order features of the velocity field are the large-scale clockwise rotation of most of the region relative to North America and the ~eastward-directed contraction along the coast arising from Cascadia subduction locking (Figure 2). The rotating region is bounded approximately in the north by the northern Basin and Range (north of and adjacent to the Snake River Plain) and the Olympic-Wallowa Lineament (OWL) extending northwest across eastern Oregon and western Washington, in the west by the Cascadia subduction zone, on the east by the Wasatch front, and in the southwest by the Walker Lane shear belt (Figure 1).

[9] Figure 4 shows the estimated strain rates and rotation rates derived from the calculated gradients in the observed velocities. We use a moving window of 2.0° × 1.6° to estimate the uniform spherical strain and rotation rates (six free parameters) every 1° of latitude and longitude by weighted least-squares [*Savage et al.*, 2001]. For each window, we first fit the data, then removed outliers with misfits exceeding three-sigma, then fit again. The overlapping windows result in smoothing of the spatial distributions of the strain and rotation rates. Any value based on fewer than five GPS velocities is not shown.

[10] The largest strain rates observed are E to ENE-directed contractions along the Oregon and Washington coasts associated with the Cascadia subduction zone, ~E-W extension along the Wasatch front and into SE Idaho to Yellowstone, and right-lateral shear along NW-trending planes in the Walker Lane shear belt of western Nevada (Figure 4a). Extension in the Basin and Range both north and south of the Snake River Plain (SRP) is evident, contrasted with the lack of strain rate within the SRP itself [*Payne et al.*, 2008, 2012]. Rotation rates are invariably clockwise except on Vancouver Island and to the north (Figure 4b). The rotation rates in a general sense increase from east to west, reaching more than 1°/Myr along the arc and forearc. As we showed earlier in MC07, these rotation rates are nearly equal to those inferred from paleomagnetic declination anomalies in the 12 to 15 Ma Columbia River Basalts [*Simpson and Cox*, 1977; *Magill et al.*, 1982; *Sheriff*, 1984; *Wells and Heller*, 1988]. Accordingly, the rotations observed with GPS over the past two decades appear to agree with those from the long term. Large rotation rates are also evident in the Walker Lane shear belt where simple shear occurs.

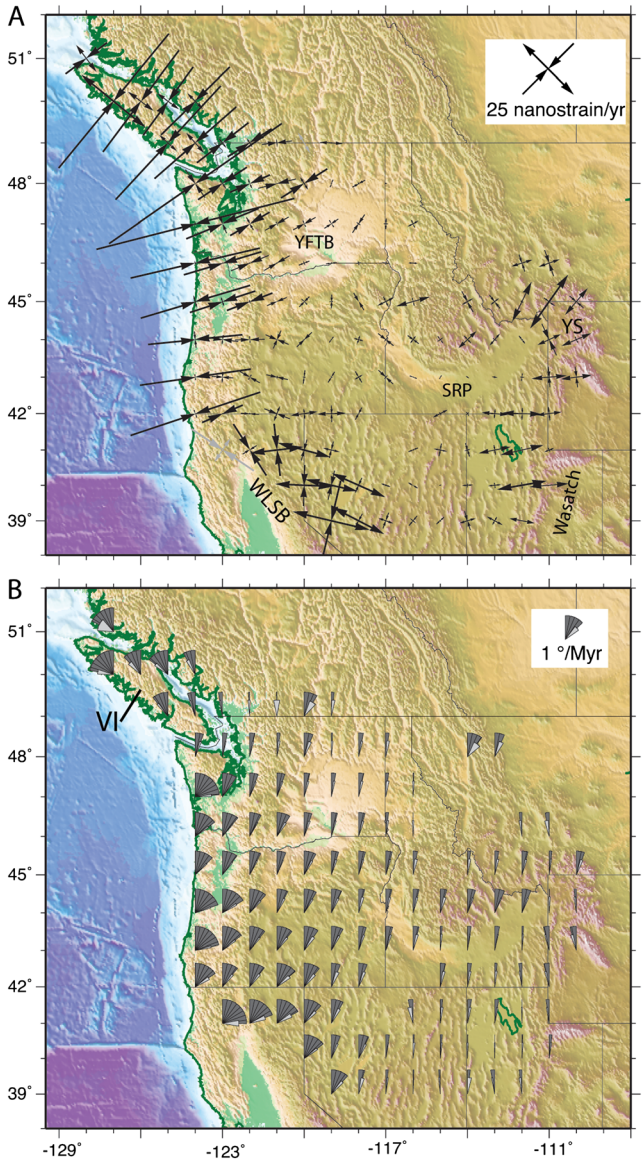

Figure 4. Principal strain and rotation rates derived from GPS velocities. Area is divided into bins of 2° (157 km) in longitude by 1.6° (178 km) in latitude in which the uniform strain and rotation rates are calculated from the GPS velocities contained within (minimum of 6 velocities). (a) Principal strain rates; scale is in nanostrain/yr (1 nanostrain/yr = 10^{-9} /yr). (b) Rotation rates for same regions. Fan symbols show the rate and sense of rotation (a fan opening 45° clockwise indicates 1°/Myr of clockwise rotation). The smaller attached fans show the one-sigma uncertainty in the rotation rate.

3. Interpretation of the Velocity Field

3.1. Update of PNW Kinematic Block Model

[11] We use the velocity field to interpret the kinematics of the PNW in terms of a series of elastic-plastic blocks that move over the surface of the Earth and are separated by active faults on which friction causes elastic deformation in the surrounding rocks (Figure 5). Block models are simple kinematic descriptions of the deformation and as such do not directly reveal the forces driving the deformation. Nevertheless, the kinematics derived from GPS velocities offer clues to the dynamics in the same manner as kinematics derived from paleomagnetic rotations and earthquake mechanisms [e.g., *McKenzie and Jackson*, 1983]. Moreover, block models provide a means to separate elastic from anelastic strain rates in the GPS velocity fields and can also be used to predict slip rates on faults without direct measurements and are thus useful for seismic hazards assessments.

[12] Here we update the block model of MC07 by inclusion of the newer GPS velocities, the addition of vertical rates derived from leveling data for the Cascadia subduction zone [*Burgette et al*., 2009], and also extend the model eastward into the Snake River Plain of Idaho by incorporating the results of *Payne et al*. [2012]. We invert the GPS velocities and other kinematic data using the program tDEFNODE [*McCaffrey*, 2009], which is an update of DEFNODE [*McCaffrey*, 1995, 2002] used in the earlier analyses. For modeling the steady state kinematics as is done here, both approaches are essentially the same. In addition to 630 horizontal and 60 vertical GPS velocities, 581 vertical rates from leveling data [*Burgette et al*., 2009] and 15 vertical rates from tide gauge data [*Dragert et al*., 1994; *Mitchell et al*., 1994; *Savage et al*., 1991], we also include 58 fault slip rates and 142 earthquake slip vector azimuths to constrain the kinematics. We exclude from the modeling those GPS velocities that have uncertainties greater than 1.0 mm/yr and set any uncertainties less than 0.2 mm/yr to 0.2 mm/yr. Many of the fault slip rates are spreading rates from the Juan de Fuca Ridge [*DeMets et al*., 2010], that constrain Juan de Fuca motion relative to the Pacific. We use North America (i.e., Stable North American Reference Frame) as the reference frame and fix the Pacific-North America rotation using the MC07 pole (longitude = 284.16°E, latitude = 50.19°N and rate = –0.761 °/Myr).

[13] In the block models, the angular velocities, internal strain rates, and fault locking parameters are estimated simultaneously by a least-squares, nonlinear inversion of all available data. In all of the inversion results presented here, we impose along strike smoothing and a penalty on the total locking on the Cascadia thrust in order to prevent locking where the data do not require it (i.e., to minimize the moment rate). The quantity minimized is

$$R^T W R + \alpha \sum_{i=1,N} \mathrm{d}^2\phi_i/\mathrm{d}x^2 + \beta \sum_{i=1,N} (\phi_i/N) + \sum P_k \qquad (1)$$

where R is the data residual matrix, W is the weight matrix, α and β are scaling factors for damping, ϕ is the locking fraction parameter that ranges from 0 to 1, x is distance in the along strike direction, N is the number of fault nodes, and P_k represents other penalties. For the runs here $\alpha = 10^6$ and $\beta = 0.2$ (based on tests of different values). The data misfit is represented by the reduced chi-square; $\chi^2_\nu = R^T W R / (N_d - N_p)$ where N_d (=2066) is the number of observations and N_p is the number of free parameters, that ranges from 112 to 174 for the models discussed. Other details of the procedure are given in *McCaffrey* [2005] and MC07.

[14] We modified the eastern side of the block model used in MC07 to coincide with that of *Payne et al*. [2012] and we combined some blocks and represent the deformation within them by a uniform strain rate tensor (Figure 5a). In particular, because we see no discrete slip across the OWL, the Yakima fold-thrust belt (YFTB) is now contained within a single block and its internal strain rate is estimated (discussed in detail later).

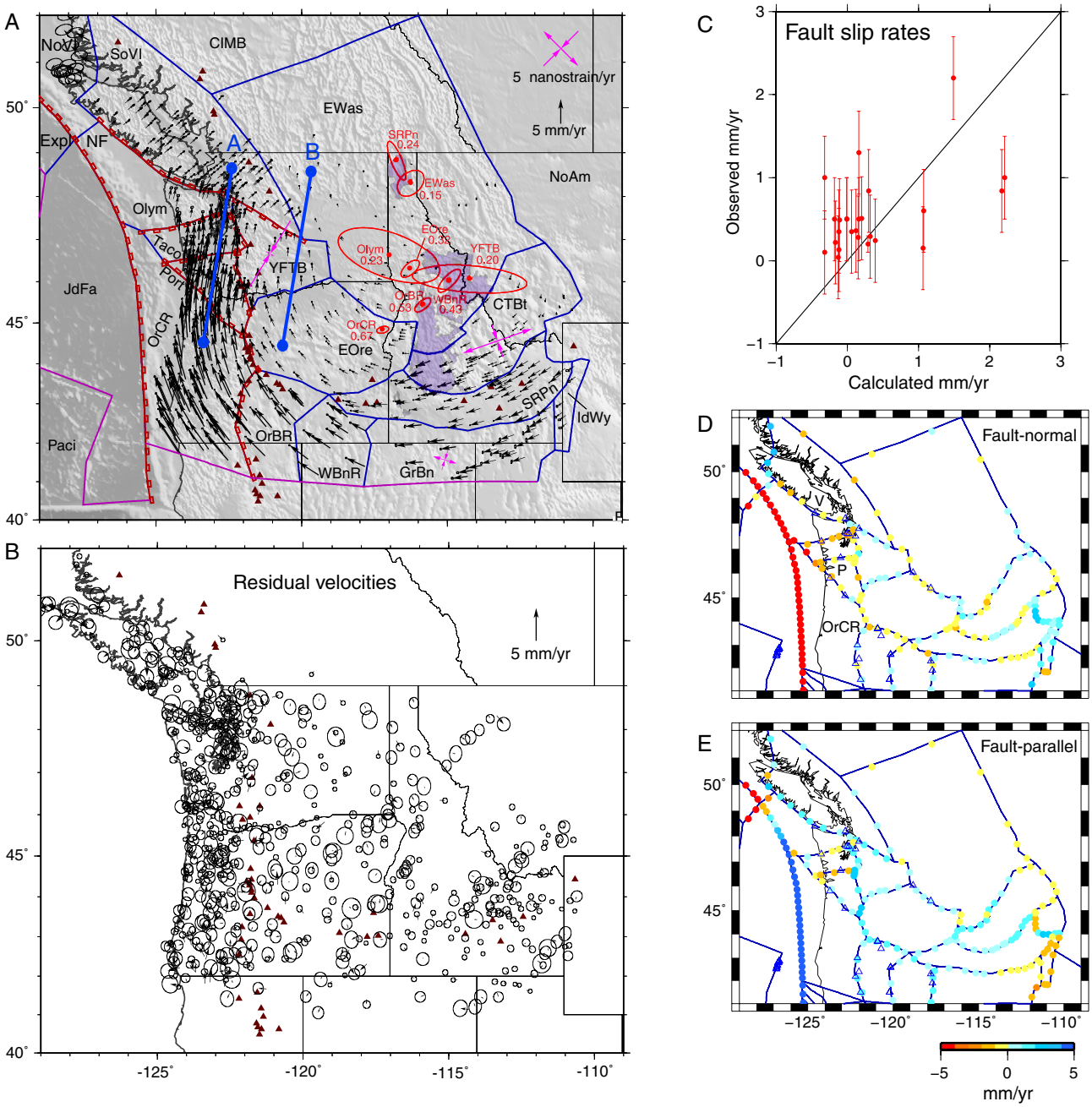

Figure 5. (a) Block model pn2d used to model GPS velocities. Blocks are designated by four-letter code. Block boundaries in red represent faults where locking was applied; teeth are on hanging wall. Blue and purple lines are free-slip block boundaries. Vectors show the velocity field after removal of elastic strain rates. Triangles are volcanoes. Line A shows baseline from Corvallis OR in the south to Bellingham WA in the north where the permanent shortening is 5.0 ± 0.5 mm/yr. Line B shows parallel baseline in the backarc where the permanent shortening is 1.9 ± 0.5 mm/yr. Also shown are poles of rotation (red ellipses are 68% confidence) and principal strain rates (purple) for the blocks (model pn2d). Poles are identified by the block code and the rotation rate in °/Myr (all are clockwise looking from above). Principal strain rates are in nanostrain/yr (= 10^{-9} /yr); scale in upper right. Shaded region is the Idaho Batholith. (b) Residual velocities from the block model pn2d, with 70% confidence ellipses. (c) Comparison of observed and calculated slip rates on crustal faults inferred from block model (pn2d). Maps of fault slip rates in their (d) fault-normal and (e) fault-parallel components (pn2d). Positive values represent normal faulting and right-lateral slip. Open triangles show locations of fault-slip rate observations. Note that the color scale is saturated at the Cascadia subduction zone.

Table 1. Fits of Cascadia Locking Models

Model	Overall χ^2_ν	Overall GPS nrms	Overall *Z* nrms	Moment Rate 10^{19} Nm/yr	SB-E GPS nrms	SB-E *Z* nrms	Notes
pn1b	1.55	1.33	0.69	12.9	1.36	0.70	Linear dropoff
pn1c	2.19	1.54	0.82	11.5	2.48	0.92	Sharp dropoff in locking
pn1d	1.44	1.30	0.61	13.4	1.48	0.65	Exponential dropoff
pn2d	1.37	1.27	0.57	7.8	1.36	0.59	Gaussian locking

Two other blocks, the Northern Basin and Range - Centennial Tectonic belt (block CTBt) and the Great Basin (block GrBn) (Figure 5a) have strain rates estimated, per *Payne et al*. [2012]. The internal strain rates are calculated in spherical coordinates [*Savage et al*., 2001] and comprise three free parameters. These parameters together with the three angular velocity parameters are equivalent to the four values in the spherical (tangential) deformation gradient tensor plus two "translation" terms (i.e., the east and north velocities tangent to the sphere).

[15] We first discuss the kinematic block model results and then evaluate the locking for Cascadia, although it should be kept in mind that these estimates are made simultaneously in the inversion runs. In MC07, we performed numerous tests of block geometries for Oregon and Washington and build on those results to assemble the geometry we use here. The various models we present in this paper differ largely in the way that locking on the Cascadia subduction thrust is parameterized.

[16] Two models that give the best fit to the data are pn1d, where full locking on the Cascadia thrust is assumed to extend to the deformation front (as was done in MC07), and pn2d, where locking is assumed to decay exponentially toward the deformation front. In both models, locking in the down-dip direction is allowed to decay with an exponential function. The χ^2_ν misfit is nearly the same for the two models (Table 1) and highlights the fact that locking near the deformation front is not constrained by the onshore geodetic data. The GPS velocities are fit with an nrms of ~1.3, which is above the expected level, but we see no systematic pattern to the residuals (Figure 5b). Geologic slip rates were fit with nrms = 1.17 and earthquake slip vectors at nrms = 1.40; both of these fits are ~20% worse than in MC07, which we attribute to the increase in the sum of the weights of the GPS data (now four times greater than in MC07) due to their increased numbers and accuracies. A model run (pn2e) excluding the vertical leveling data and without smoothing of the Cascadia locking distribution reduced the GPS nrms only slightly, to 1.24, indicating that the GPS and vertical data are compatible and that the locking model is not overly smoothed. We tried elevation corrections using a Varying Depth model [*Williams and Wadge*, 1998], where the depth to dislocation sources is the vertical distance from the GPS site to source, but that did not reduce the misfit. The nrms of the GPS within blocks seemed to increase toward the coast suggesting that the misfit may increase with larger strain rates (model error) or with increased atmospheric moisture (data error) near the coast. The vertical data from *Burgette et al*. [2009] are fit with nrms ~ 0.60 suggesting their uncertainties might be overestimated (uncertainties are taken from Burgette et al. without rescaling). The locking models are discussed in detail later.

[17] Internal strain rates are estimated for three of the regions (Figure 5a): YFTB, CTBt, and GrBn. In other blocks internal strain rates either did not contribute to the deformation, in the sense of providing a better fit to the data, or traded off with the elastic strain rates. In the forearc block OrCR, a N-S contraction rate of −3.4 nanostrain/yr (1 nanostrain/yr = 10^{-9}/yr) resulted when it was estimated, which is consistent in orientation with seismicity [*Wang*, 1996], but well below the ENE-directed elastic contraction rate of ~100 nanostrain/yr and may not be a resolvable feature in this setting. In the YFTB, NE-directed contraction dominates, as discussed in detail below. The strain rates in the CTBt and GrBn are showing Basin and Range extension with some component of shear, as discussed by *Payne et al*. [2012].

[18] The block model estimates slip rates on the block boundaries that are used to represent slip on faults. The observed fault slip rate constraints are matched reasonably well (Figure 5c) but most of the rates on crustal faults are low (< 2 mm/yr) (Figures 5c, 5d, and 5e). Slip rates on the faults within the forearc are not well-constrained by the GPS data due to their low rates and the high strain rates produced by subduction. East of the arc, where subduction strain rate is lower, until the Wasatch front and northward to Yellowstone, we see no indications of fault slip rates exceeding ~2 mm/yr. The majority of the relative motion from the east to west is accommodated by rotation (Figure 5a). Permanent shortening (i.e., with the elastic component removed) between Corvallis, OR in the forearc and Bellingham, WA is 5.0 ± 0.5 mm/yr (Figure 5a western profile) taken up by contraction across faults between Portland, OR and Seattle, WA (Figure 5e). North-south shortening in the backarc is considerably less, 1.9 ± 0.5 mm/yr along the eastern profile line in Figure 5a, indicative of the predominant role of rotation about nearby poles to the east.

[19] The well-determined poles of rotation for the blocks cluster in the region of northern Idaho near the Idaho Batholith, invariably showing clockwise rotation (Figure 5a; poles are not shown for blocks that have very large uncertainties). The rotation rates, relative to North America, show a decrease eastward away from the coast; the highest rate (0.66 ± 0.02 °/Myr) is for the Oregon Coast ranges block and decrease to about half that rate in Eastern Oregon (0.32 ± 0.02°/Myr) and about one third in the Snake River Plain (0.24 ± 0.01°/Myr). The eastward decrease in rotation rates is also seen in paleomagnetic rotations [*England and Wells*, 1991]. The geodynamic implications of the rotations are discussed in section 3.6.

3.2. Cascadia Subduction Locking

[20] *Hyndman and Wang* [1993] and *Fluck et al*. [1997] inferred locking on the Cascadia subduction zone from models of interface temperature and such a model was consistent with observations of vertical motions from leveling at the time. They suggested that locking is confined to the offshore in both the Oregon and Vancouver Island sections of the subduction zone but extends beneath the coast of the Olympic Peninsula. Several more recent models have been developed using

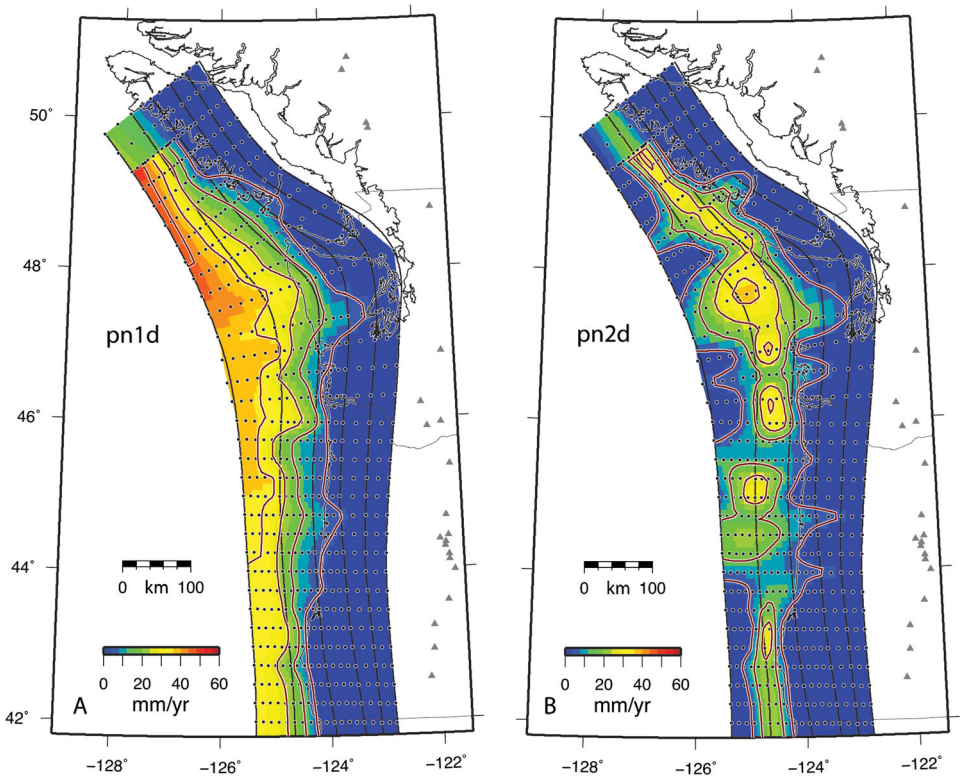

Figure 6. Locking model results for two parameterizations of locking (see text for functions). Colors and contours are of the slip deficit rate, in mm/yr. Slip deficit rate contours are 5, 15, 25, 35, and 45 mm/yr. (a) Tapered transition zone of variable width, depth, and taper but locked to trench (pn1d). (b) Gaussian distribution of locking with depth (pn2d).

horizontal GPS velocities only [*McCaffrey et al*., 2000; *Wang et al*., 2003], using vertical leveling data only [*Burgette et al*., 2009], or using both horizontal and vertical GPS (MC07). *Burgette et al*. [2009] suggested that there is a disagreement between the horizontal GPS and vertical leveling data though they did not try to fit the GPS. We show below that both data sets can be satisfied by a common locking model.

[21] The Cascadia plate interface geometry is based on the slab contours of *McCrory et al*. [2003], the same geometry we used earlier and by *Burgette et al*. [2009]. The methodology for the subduction model we use is described in detail in MC07 (see their section 4.3). The convergence of the Juan de Fuca plate with the forearc is estimated simultaneously with the locking parameters and is constrained also by Juan de Fuca spreading rates relative to a fixed Pacific-North America pole. Because our block model has changed only in detail from that of MC07, here we will focus on the effects of including the vertical leveling data in constraining Cascadia locking.

[22] The Cascadia plate interface is represented by node points (longitude, latitude, and depth) that recreate its three-dimensional geometry (Figure 6). The nodes form 34 profiles in the downdip direction from the southern end (40.5°N) to the northern end (49.3°N) of the section of Cascadia where the Juan de Fuca plate subducts. The spacing between these profiles is approximately 40 km along strike. To the north of the Nootka Fracture Zone an additional fault section is used where the Explorer Plate thrusts beneath northern Vancouver Island (Figure 5a). The nodes are placed at depth every 2 km in the upper 20 km, every 2.5 km from 20 to 30 km depth and then every 5 km down to 50 km depth. Locking is applied by using backslip in an elastic half-space at each node and convolving it with precalculated Greens functions (based on *Okada* [1992]) that give the surface responses (at observation sites) to slip at the nodes. In the inversion, the fraction of locking, called ϕ, at the nodes is estimated and then backslip is applied at $-\phi V$ where V is the slip velocity, derived from the relative block rotations across the fault. The product ϕV is often called the slip rate deficit.

[23] The variation in $\phi(z)$ with depth at the nodes is assigned by two different functions, both with three free parameters; a scale A or γ, and two depths Z_1 and Z_2: (1) a Gaussian function where $\phi(z) = A \exp\{-1/2 [(z - Z_1) / Z_2]^2\}$; and (2) the function introduced by *Wang et al*. [2003] and modified by MC07 (their equation (3) and Figure 7a). For function (2), locking is full ($\phi = 1$) at depths less than an upper depth Z_1, free slip ($\phi = 0$) occurs below a lower depth Z_2, and from Z_1 down to Z_2, ϕ drops from 1 to 0 according to a function whose form is determined by the parameter γ (see MC07 Figure 7a). The second function imposes locking out to the trench while the first merely allows it. The section of the fault between Z_1 and Z_2, where locking decreases with depth, is commonly referred to as the transition zone.

[24] *Burgette et al*. [2009] suggested that inversions based on only GPS data or only vertical data result in different estimates of the transition zone width. In particular, along the central Oregon section (~44.6°N) of the coast, uplift is slow, which has been explained by either a wide transition zone extending beneath the coast (MC07) or a narrow one entirely offshore [*Burgette et al*., 2009]. We ran inversions to test whether or not the combined vertical leveling and horizontal

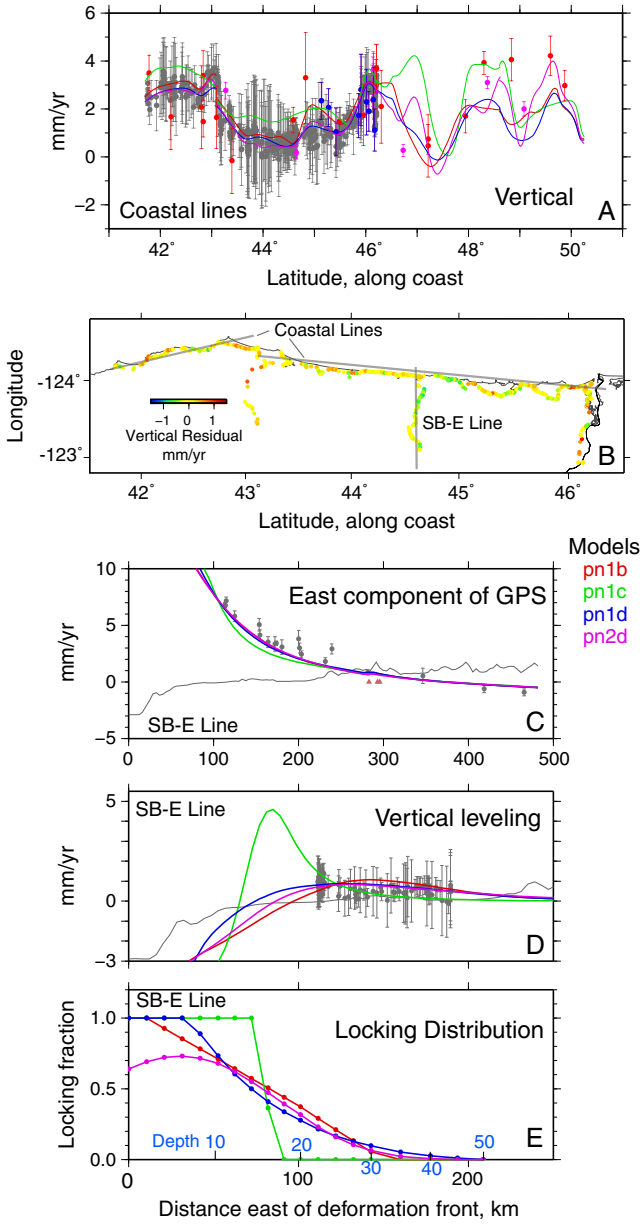

Figure 7. (a) Uplift rates in south-to-north profile along the coast. Gray symbols are observations from leveling, purple from tide gauges, red from continuous GPS and blue from survey GPS; error bars are one-sigma. Curves are predicted from models, coded by color. Sites plotted are within 50 km of the profile line. (b) Map of residuals of vertical leveling rates along Oregon coast (model pn2d). Gray lines show location of profile SB-E (Figures 7c–7e) and coastal profile (Figure 7a). Profile of locking and fits to data across the Cascadia subduction zone at 44.6°N, line SB-E, where uplift rates are low, for four models discussed in the text. (c) East component of the GPS velocities, error bars are one-sigma; (d) uplift rates from leveling [from *Burgette et al.*, 2009] error bars are one-sigma; (e) locking fraction profiles (1.0 indicates fully-locked and 0.0 is freely-slipping). Gray lines show the topographic profile (in km, based on mm/yr scale), triangles show the volcanic arc and the coast is at the westernmost observation point. Colored curves show the model predictions.

GPS observations can be matched with a common locking distribution and whether they indicate a narrow or broad transition zone. We find that both the horizontal GPS and vertical leveling data are fit better with a broad transition zone beneath the central Oregon coast.

[25] Inversions in which the transition zone is constrained to be narrow by forcing a sharp drop off in the exponential transition (function 2, setting $\gamma = 0.1$; pn1c) result in the misfit reduced chi-square $\chi^2_\nu = 2.19$ (Table 1 and auxiliary material). Run pn1c is similar to the approach used by *Burgette et al.* [2009], using function (2) where γ is fixed and Z_1 and Z_2 are adjusted along each of the profiles. In run pn1b we fixed γ at 5.0, which results in a linear drop in ϕ across the transition zone, and solved for the upper and lower depths; resulting in $\chi^2_\nu = 1.55$. Allowing, but not enforcing, a broader transition zone using the Gaussian locking distribution (function 1) results in a lower $\chi^2_\nu = 1.37$ (pn2d) and a better fit to both the vertical and horizontal data (Table 1). Finally, we solved for γ and both upper and lower depths (pn1d), resulting in $\chi^2_\nu = 1.44$. In general, the broad transition zone solutions fit both the GPS and leveling data better than the narrow transition zone models (Table 1). The better fit of pn1d (γ free) relative to pn1b (γ fixed so $\phi(z)$ is linear) is significant at a 97% level based on an *F*-test and the addition of 31 free parameters to pn1d; hence, the decay in locking with depth across the transition zone is more likely to have some curvature than being strictly linear.

[26] Our preferred locking models pn1d and pn2d (Figure 6) match the along strike variations in vertical rates (Figures 7a and 7b) including the low uplift rates in central Oregon. Published locking models [*Fluck et al.*, 1997; MC07; *Burgette et al.*, 2009] differ in the region off central Oregon, around 44.6°N, where tide-gauge uplift rates are near zero [*Mitchell et al.*, 1994]. MC07, from GPS and sparse vertical data, inferred a broad transition zone that extended below land while *Burgette et al.* [2009], from vertical data alone, inferred a narrow transition zone offshore. To look at this discrepancy in detail, for the locking models (Table 1), we calculated the nrms misfits to the horizontal GPS and leveling data along the SB-E line of *Burgette et al.* [2009], a line running eastward from the coast at Newport, Oregon, where uplift rates are small (Figure 7 and Table 1). We used 24 GPS velocities and 126 uplift rates within 25 km of the profile to compare fits. For the model (pn1c) that used a sharp drop-off in locking (narrow transition zone; Figures 7c–7e), the nrms for the GPS and leveling data are 2.48 and 0.92, respectively. For the other three models that include a broader transition zone (Figure 7e) the nrms are ~1.4 and ~0.6 to 0.7 for GPS and leveling, respectively (Table 1). Accordingly, we conclude from the better fits to both GPS and leveling data that the central Oregon section of the Cascadia subduction zone exhibits a broader transition zone than to the south.

[27] The locking inferred from geodetic data allows estimates of the minimum and maximum rates of moment accumulation. Using the minimum locking constraint and Gaussian slip distribution, where locking does not extend to the trench (pn2d), gives a moment rate of ~8×10^{19} Nm/yr. A magnitude M_w 9.0 earthquake has a moment of 4.0×10^{22} Nm, which could build in ~500 years at the current rate. Note that our velocities have already been corrected for the release of moment in slow-slip events so these locking rates represent the decade-scale average.

[28] While it is generally thought that earthquake rupture does not extend to the deformation front, there is evidence that it did so in the 2011 Tohoku-oki earthquake [*Fujiwara et al.*, 2011]. Using function (1) where locking extends to the trench, the moment rate for the model pn1d is ~13 × 10^{19} Nm/yr, or about 50% more than the minimum. Hence, at this rate, the return time for a M_w 9 would be about 300 years if all the moment were released in a single event. These return times are comparable to the observed average time (~500 years) between large earthquakes in Cascadia [*Goldfinger et al.*, 2012] but it should be emphasized that both the return times and moment rate calculations are highly uncertain and should not be used for predictive purposes.

3.3. Yakima Fold-thrust Belt

[29] The YFTB lies east of the Cascades of Washington and Oregon along the southeastern continuation of the OWL [*Raisz*, 1945], a crustal fracture that extends along the YFTB and westward into the Puget Lowlands region (Figure 1). The folds and faults of the YFTB deform the youngest Columbia River Basalt as well as Miocene to Pleistocene sedimentary rocks that overlie them. The deforming region comprises asymmetrical, ridge-forming anticlines separated by valleys 10–20 km across [*Reidel et al.*, 1989, 1994; *Yeats*, 2012] and the folds appear to be controlled by thrusts, many of which are blind [*Yeats*, 2012]. The Toppenish Ridge, Saddle Mountains, Umtanum Ridge, and Manastash Anticline structures have revealed evidence of Holocene deformation [*Campbell and Bentley*, 1981; *Reidel et al.*, 1994; *West et al.*, 1996; *Ladinsky et al.*, 2010; *Blakely et al.*, 2011]. *Reidel et al.* [1994] estimate that the folds have accommodated at least 15 to 25 km of shortening and faulting up to 4 km in the last 10.5 Myr along longitude 120 W. *Blakely et al.* [2011] suggest a possible connection of faults of the YFTB through the Cascade arc to the Southern Whidbey Island fault within the highly populated Puget Sound region (Figure 8). If so, it forms a continuous system that includes the western Rattlesnake Mountain and Umtanum Ridge faults (Figure 8) forming a 200 km long fault zone capable of a magnitude 7 or larger earthquake.

[30] The region has distributed earthquake activity that appears to be elevated relative to surrounding regions (Figure 8), except to the northwest in the Puget Sound region [*Ludwin et al.*, 1991; *Gomberg et al.*, 2012]. Most seismicity is shallow, less than 4 km, but some is as deep as 25–30 km, and swarms are common. Focal mechanisms show predominantly reverse and strike-slip motion on E- and NW-striking faults, consistent with orientation of the YFTB structures.

[31] The YFTB has a westward-broadening morphology consistent with fan-like closing about a pole to the southeast (Figures 1 and 8). The deformation rate across the YFTB has been difficult to estimate from geologic studies of active faulting but some idea of the active deformation can be gleaned from our GPS velocities. To estimate the geodetic deformation, we take a region encompassing the YFTB and estimate the rotation rate and uniform horizontal strain rate from the 55 GPS velocities within it in the same manner described above for Eastern Oregon (Figure 9). The rotation axis falls to the east, along the OWL (Figure 9a) and the average strain rate tensor has its maximum contraction rate of –6.8 ± 0.5 nanostrain/yr in a NE direction (Figure 9b) (56° ± 4° east of north), which is more northerly than the subduction-induced contraction seen farther west in the coastal regions (Figure 4a). The direction of this contraction rate is nearly perpendicular to the OWL, indicating little if any shear occurs along it. When the strain rates in the YFTB are estimated separately for the regions SW and NE of the OWL, they are very similar to each other and to the average (–7.7 ± 1.3 nanostrain/yr at 72° ± 8° to the NE and –7.0 ± 0.9 nanostrain/yr at 60° ± 6° to the SW of the OWL). Hence, despite the notable change in orientations of the ridges on either side of the OWL, the modern strain rate does not change measurably. Profiles in Figures 10a and 10b, nearly perpendicular to the OWL, show that there is no discernible change in velocity across the OWL in either the parallel or normal direction. Hence, the OWL does not at present seem to be a focus of the deformation in the YFTB. Our earlier model in MC07 placed 1 to 2 mm/yr of oblique shortening across the OWL but we now suggest based on better velocities that this slip is distributed across the YFTB structures rather than being localized. *Pratt* [2012] suggests that the current YFTB structure is inherited from earlier strike-slip movement on the OWL that may not be active at present.

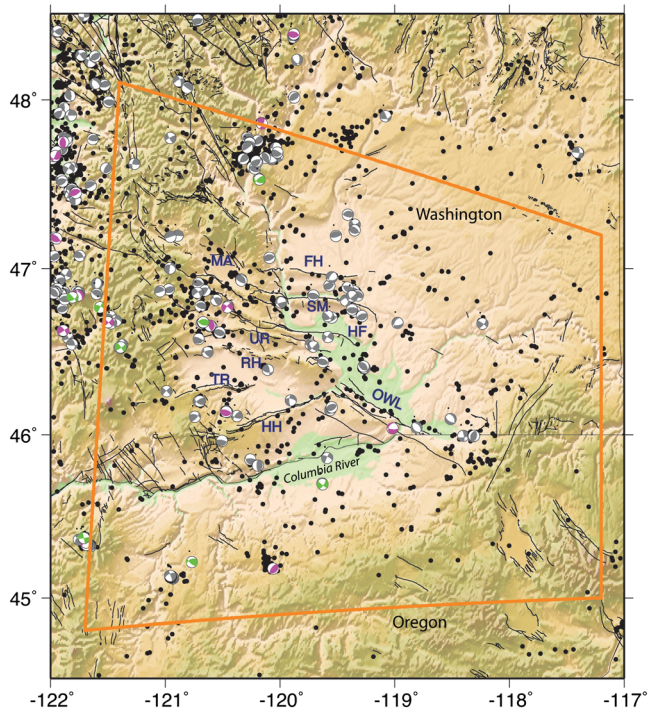

Figure 8. Map of seismicity and focal mechanisms near the Yakima fold-thrust belt (YFTB). Dots – epicenters taken from Advanced National Seismic System from 1980 to April 2011 (http://www.ncedc.org/anss/), where depth is less than 40, magnitude greater than 2. Colored focal mechanisms are compiled from several sources (listed in *McCaffrey et al.* [2007]) and gray-filled are from Pacific Northwest Seismic Network ($m_b \geq 3$). Colored box outlines study region. Gray lines show locations of suspected faults. OWL – Olympic-Willowa Lineament, FH – Frenchman Hills, SM – Saddle Mountains, UR – Umtanum Ridge, RH – Rattlesnake Hills, TR – Toppenish Ridge, HH – Horse Heaven Ridge, MA – Manastash Anticline.

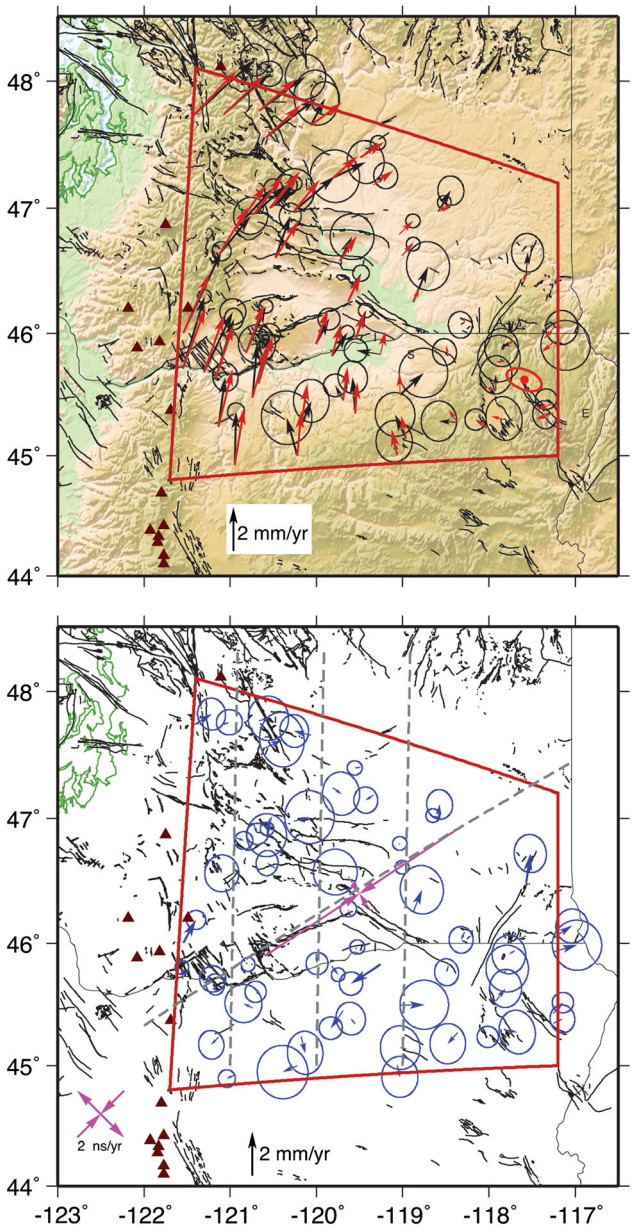

Figure 9. (a) Observed (black) and predicted (red) GPS-derived velocities within the Yakima fold-thrust belt, relative to North America. Only those with uncertainties of less than 0.8 mm/yr are shown (error ellipses are at 70% confidence level). The pole of rotation is red ellipse in lower right corner of region (rotation is clockwise at –0.35°/Myr). (b) Residual velocities after removing a rotation and uniform horizontal strain rate from the velocities shown in Figure 9a. The resulting strain rate is shown by purple arrows near the center. Gray dashed lines are the profiles shown in Figure 10.

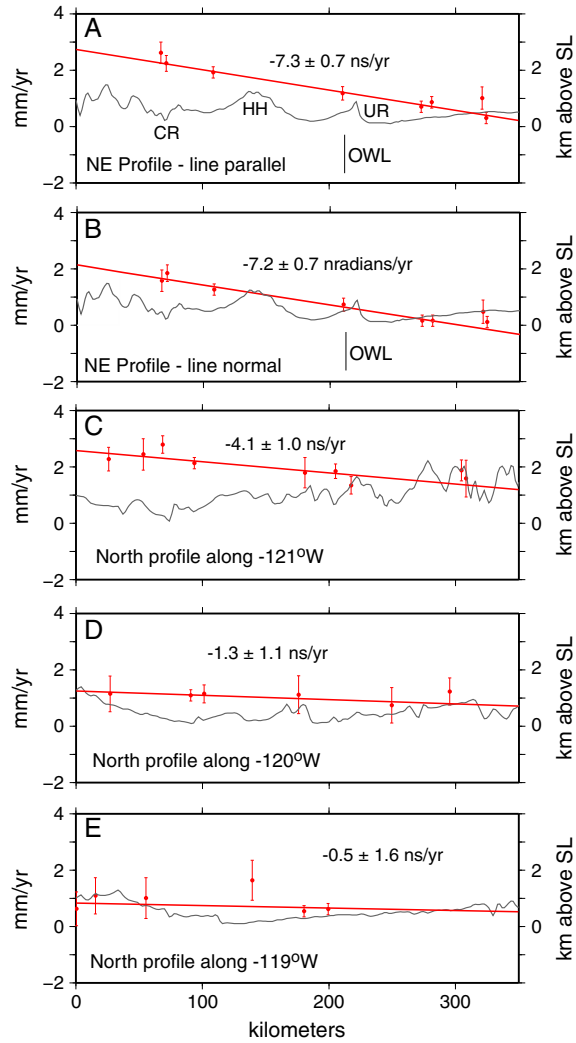

Figure 10. (a) SW to NE profile of NE-components of GPS velocities (with one-sigma error bars) crossing the YFTB (profile location in Figure 9B). Red line is the best fit slope and gives the contraction rate in nanostrain/yr (ns/yr). Gray curve shows elevation along profile (scale to right). (b) Same profile as in (a) but showing the NW-components of the GPS. CR – Columbia River, HH – Horse Heaven Ridge, UR – Umtanum Ridge. South-to-north profiles across YFTB at (c) −121°W, (d) −120°W, and (e) −119°W. The eastward decrease in the N-S strain rate is consistent with the YFTB closing like a fan about a pole to the east.

3.3.1. Stress Inversion

[32] Using 424 earthquake focal mechanisms from the Pacific Northwest Seismic Network we estimate the directions of stress within the Yakima fold-thrust belt. Earthquakes are from 1970 through June 2006 in the region enclosed in the polygon in Figure 8 and their magnitudes are greater than 1.0. We used the software SATSI [*Hardebeck and Michael*, 2006] that finds the best fit uniform stress tensor to explain the senses of slip in the compilation of earthquakes. The resulting trend of the most compressive stress was between 4° and 12° east of north with a plunge of 3 to 13° (ranges are 95% confidence based on bootstrap error estimate using 1000 resamplings). The least-compressive stress is steep (57° to 80° plunge) and the intermediate stress is nearly E-W (azimuth of 95° to 106°) and nearly horizontal (6° to 30° plunge). The ratio of the stresses $\sigma_2 - \sigma_3 / \sigma_1 - \sigma_3$ (where σ_1 is the most compressive stress and σ_3 the least) ranged from 0.1 to 0.4. Hence the stress derived from earthquake mechanisms is revealing ~N-S contraction and vertical extension (crustal thickening).

3.3.2. Moment Tensor Summation

[33] From the same set of earthquakes we used a *Kostrov* [1974] seismic moment summation to estimate the seismic

strain rate tensor. Assuming a crustal area of 100,000 km^2 (Figure 8), 10 km thick and a rigidity of 40 GPa, the seismic strain rate is –0.03 nanostrain/yr (contraction) at N3°E and orthogonal extension at 0.01 nanostrain/yr (plus 0.02 nanostrain/yr of crustal thickening assuming incompressibility). By comparison, the N-S geodetic contraction rates across the YFTB from our GPS observations are –4.1 ± 1.0 nanostrain/yr along −121°W (Figure 10c), –1.3 ± 1.2 nanostrain/yr along −120°W (Figure 10d) and –0.5 ±1.5 nanostrain/yr along −119°W (Figure 10e). The N-S geodetic strain rates decrease to the east, as expected if Oregon is rotating clockwise into Washington about a nearby pole to the east.

[34] The seismic strain rates are ~2 orders of magnitude lower than the geodetic rates. This difference may indicate that the strain in the YFTB is largely aseismic or that there is considerable moment deficit rate that might be leading to a large earthquake. The annual moment rate from the seismicity is 2.1×10^{15} Nm/yr and the moment accumulation rate inferred from the geodetic strain rate should be about 100 times that, or about 2×10^{17} Nm/yr. Put another way, the current seismicity produces an equivalent of an M_w 4.1 earthquake per year while the geodetic strain rate indicates the moment rate of an M_w 5.4 per year. The modern geodetic moment accumulation rate is roughly equivalent to a magnitude 7 earthquake (4×10^{19} Nm) every 200 years. The largest known earthquake in or near the YFTB was the 1872 $M \sim 6.8$ event of unknown mechanism near Lake Chelan at the northern edge of the thrust belt [*Bakun et al.*, 2002]. The largest in instrumental times was an M_w 5.7 in 1980.

3.4. Implications for Low Strain Rates in Eastern Oregon

[35] A currently controversial question concerning our understanding of continental dynamics is the relative importance of forces acting on the sides of the continents, internal density variations and basal forces. Related questions are what controls the strength of continental lithosphere (crust or mantle) and what is the stress level on crustal faults? One view of continental deformation holds that flow in the viscous mantle determines the surface tectonics in a broad sense—the rigid surface plates move along with the mantle, responding to basal stress, but do not exactly mimic the mantle flow. To accommodate the motion, the brittle crust breaks into quasi-rigid blocks separated by faults. Hence, block models that require many small blocks to fit the observations are comparable to continuum deformation.

[36] Recent seismological experiments in eastern Oregon show that it has a relatively thin crust and a warm upper mantle [*Eagar et al.*, 2011; *Gilbert*, 2012]. Shear-wave splitting results show consistent east-west fast-splitting orientations throughout the region, presumably revealing ~ east-west mantle flow [*Xue and Allen*, 2006; *Long et al.*, 2009]. Accordingly, any surface velocities driven by the basal tractions arising from mantle flow should be eastward or westward but could have gradients in either the east or north directions or both.

[37] To examine the possible effect such flow might have on the crust of eastern Oregon, we estimate its angular velocity and average strain rate from our GPS velocity field. If the region is undergoing simple shear, possibly driven by mantle flow, the rotation and shear strain rates should be approximately equal in magnitude. The region examined (Figure 3) is about 700 km north-to-south and about 400 km east-to-west, bounded by the Brothers Fault zone in the south, Yakima fold-thrust belt in the north, the volcanic arc to the west and the Snake River Plain to the east, and contains 89 horizontal GPS velocities with uncertainties less than 0.8 mm/yr. The Cartesian deformation rate gradient tensor derived from the velocities is:

$$\begin{vmatrix} \mathrm{d}Vx/\mathrm{d}x & \mathrm{d}Vx/\mathrm{d}y \\ \mathrm{d}Vy/\mathrm{d}x & \mathrm{d}Vy/\mathrm{d}y \end{vmatrix} = \begin{vmatrix} -1.8 & 8.3 \\ -6.5 & -1.6 \end{vmatrix} \times 10^{-9}/\mathrm{yr}$$

where x is east and y is north. That the off-diagonal terms are large and nearly equal in magnitude but opposite in sign shows that this is largely a rigid-body rotation and not simple shear (the rotation rate is 1/2 the difference in these values, while the shear strain rate is 1/2 their sum). The pole of rotation falls at the northeastern edge of the region with a rotation rate of 0.43 ± 0.01 °/Ma (~7.3 ± 0.2 nanoradians/yr). The rotation results in a change in the azimuth of the GPS velocities in excess of 90° from the southeastern to northwestern edge of the area (Figure 2a). The principal horizontal strain rate tensor is entirely contraction; -2.7 ± 0.3 nanostrain/yr at $129 \pm 8°$ azimuth and -1.0 ± 0.3 nanostrain/yr in the orthogonal direction (some part of this contraction is undoubtedly elastic, due to Cascadia subduction). This calculation demonstrates that most of the velocity gradients across eastern Oregon are due to rotation rather than shear strain.

[38] The rigidity and rotation of surficial eastern Oregon may be at odds with the seismological inferences of a deforming mantle, unless the lithosphere and underlying mantle are dynamically decoupled in the sense that the stress acting on the base of the lithosphere is not sufficient to cause significant deformation in it. Mantle flow at the base of the lithosphere leads to stress acting at the boundary, which must be balanced by stress gradients within the lithosphere. The continuum concept of continental dynamics holds that the crust is not strong enough to maintain these stress gradients over long distances and times. The velocity change across the 400–500 km of eastern Oregon is about 4 mm/yr from south to north, but is predominantly accommodated by rotation rather than strain. If the mantle is shearing as much as the seismological evidence might indicate, the lack of surface deformation suggests that the stress between the crust and mantle is small, or that the crust is strong. The existence of internal crustal strength may be indicated by the elevation of the eastern Oregon plateau (~1 km above sea level) and the absence of ongoing collapse.

[39] *Humphreys and Coblentz* [2007] evaluated the relative importance of forces acting on the North American continent and concluded that basal stress was relatively small compared to bounding stress (on faults) and internal forces from lateral density variations (giving rise to lateral forces from gravitational potential energy gradients). The rotation of eastern Oregon results in surface velocities that change by more than 90°, hence it is likely that the mantle resists this motion at least beneath part of it. Gravitational potential energy variations alone cannot drive such a rotation. Hence, we conclude that eastern Oregon supports the concept that crust in some continental regions is strong relative to the mantle [i.e., *Jackson*, 2002] and that edge forces are driving its rotation. One possibility for its strength is that the crust/lithosphere of eastern

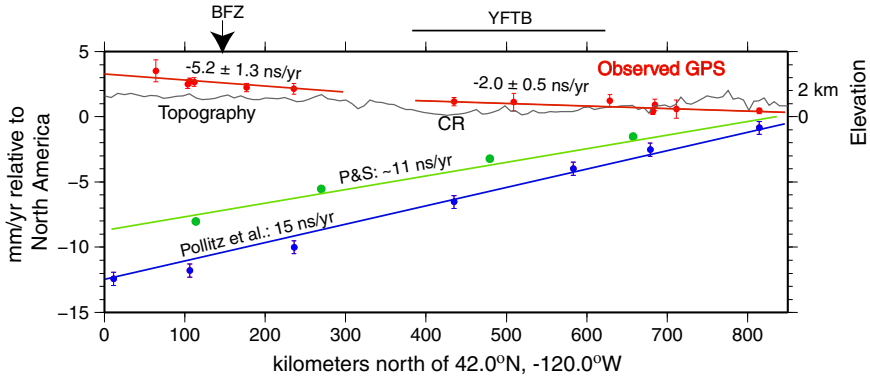

Figure 11. South-to-north profile across the region along −120°W, starting in the south at 42°N. Red dots show observed GPS velocities with one-sigma uncertainties. Blue dots are from *Pollitz et al.* [2010] (velocities from their Figure 12A) and green are from *Puskas and Smith* [2009, Figure 6], representing time-dependent velocities due to postseismic mantle relaxation following the 1700 Cascadia and other earthquakes. Lines through the dots are approximate best fit strain rates in 10^{-9} /yr (ns/yr); positive is extension; negative is contraction. Gray curve shows topography; scale to right. BFZ is the location of the Brothers Fault zone (Figure 1), YFTB is the Yakima fold-thrust belt; CR is the Columbia River.

Oregon has been under-plated by the subducted Siletz terrane [*Schmandt and Humphreys*, 2011]. In a similar fashion, addition of volcanic material to the crust of the Snake River Plain may explain its geodetic rigidity also in the presence of a warm upper mantle [*Payne et al.*, 2012].

3.5. Postseismic Mantle Relaxation

[40] The low strain rates evident in eastern Oregon are also at odds with notions that the current PNW surface velocity field includes a large, time-dependent signal due to the viscoelastic response of the mantle and crust to past earthquakes [e.g., *Puskas and Smith*, 2009; *Pollitz et al.*, 2010]. *Pollitz et al.* [2010] proposed that the modern velocity field is due to the summation of time-dependent viscoelastic relaxation due to recent earthquakes, time-independent (cycle-averaged) relaxation from past earthquakes and time-independent fault creep. The time-dependent component of their velocity field (their Figure 12A) in the PNW region is largely due to mantle relaxation following the 1700 A.D. earthquake on the Cascadia subduction zone. The current predicted component of the velocity field due to that relaxation shows N-S extension across eastern Oregon and Washington at a rate of ~15 nanostrain/yr (~12 mm/yr change in north component of velocity over ~800 km from 42°N to 49°N along −120°W; Figure 11). *Puskas and Smith* [2009] made a similar correction that added a N-S extension rate of ~11 nanostrain/yr (Figure 11). Since the present GPS measured field reveals a N-S contraction rate that is about 2 to 5 nanostrain/yr along the same profile (Figure 11), the long-term time-independent strain rate field must cancel and exceed these proposed transient signals at the present time. In other words, the *Pollitz et al.* [2010] model requires ~15 mm/yr of steady state N-S shortening in eastern Oregon and Washington to match the modern GPS observations The *Puskas and Smith* [2009] correction adds a N-S extension of 12 mm/yr that implies a similar amount of permanent shortening. Moreover, this shortening must be distributed rather than localized because it has to cancel out the long wavelength mantle relaxation signal (Figure 11). Apart from the Yakima fold-thrust belt that may accommodate up to 3 mm/yr N-S shortening [*Reidel et al.*, 1994] and the Brothers Fault zone that could account for 1 or 2 mm/yr [*Bird*, 2009], there are no obvious geologic structures to take up the 12 to 15 mm/yr relative motion in the Oregon and Washington backarc [*Wells et al.*, 1998]. In addition, the agreement of the modern GPS-derived rotation rate of eastern Oregon with the long-term average rate from paleomagnetic observations [*Simpson and Cox*, 1977; *Magill et al.*, 1982; *Sheriff*, 1984; *Wells and Heller*, 1988; MC07] suggests that the present field is similar to its steady state and any transient signals in the PNW must be small. Similarly, *Payne et al.* [2012] modeled the 1983 Borah Peak, Idaho *M* 6.9 and 1959 Hegben Lake, Montana *M* 7.3 earthquakes and found that any postseismic relaxation from them has very little influence on the modern GPS velocities. We suggest that the presence of a slowly-straining, rotating region is a simpler explanation for the modern velocity field of eastern Oregon than the near-cancellation of two very large strain rates, one steady state and one time-dependent. The lack of a large postseismic transient signal in the PNW may be attributed to a different viscosity structure or smaller slip during the modeled earthquakes than assumed by *Puskas and Smith* [2009] and *Pollitz et al.* [2010].

3.6. Geodynamic Implications for Large-scale Rotations of the Pacific Northwest

[41] In their analysis of North American deformation, *Humphreys and Coblentz* [2007] suggested that the main driving forces were bounding stresses and internal density (gravitational potential energy) differences and that basal shear played a minor role. Compression of the eastern US is largely due to ridge push of the North Atlantic spreading center and mantle flow above the sinking Farallon slab while extension in the west is from gravitational collapse and cratonic root drag. In addition, shear from the Pacific-North America motion likely contributes to deformation in the southwestern U.S. [*Atwater*, 1970; *McCaffrey*, 2005; *Flesch et al.*, 2007; *Parsons and Thatcher*, 2011].

[42] Deformation of the upper, continental plate in the Pacific Northwest (PNW) takes up only a small portion of

the Pacific-North America relative plate motion compared to south of the MTJ where nearly all deformation is within the continent. Moreover, the motion of the PNW appears to be accommodated to a large degree by crustal rotations, whereas to the south, crustal faulting predominates.

[43] The cause of the crustal rotations in the PNW is not entirely clear. In California, the vertical-axis rotation (spin) rates of blocks, in the North America frame, generally fall between that of the Pacific (~0.7°/Myr clockwise) and zero (the spin rate of North America) suggesting that they spin in response to Pacific-North America shear, either through coupling with the mantle or block-to-block transmission of velocity gradients [*McCaffrey*, 2005; *Parsons and Thatcher*, 2011]. The spin rate of the Juan de Fuca plate, is –1.3°/Myr clockwise near the Cascadia subduction zone, and the apparent eastward decrease in spin rates in the crustal blocks (Figure 5a) suggests a similar relationship. The clockwise spin of the Juan de Fuca plate results in a south-to-north increase in the convergence rate along the Cascadia subduction zone. If the stress acting on the subduction fault increases in some way with convergence rate, then a clockwise torque may be applied to the coasts of Oregon and southern Washington contributing to the rotation of the Oregon Coast Range. However, such a torque might be expected to produce a block rotation axis close to the forearc, where the force is applied, rather than hundreds of kilometers inland, where it is observed (i.e., near the Idaho Batholith), so we suspect that subduction alone is not driving the rotations. Instead, a large-scale rotation consistent with right-lateral Pacific-North America shear, with stresses acting across block boundaries, could be driving the clockwise rotations. The rotation of the Oregon forearc, for example, is modified by forces applied at its nonsubduction edges. In the absence of these other forces the forearc would spin at the same rate as the Juan de Fuca plate. In the south, in the Walker Lane shear belt, right-lateral shear along NW-trending zones [*Hammond et al*., 2011] produces velocity gradients that would add a component of clockwise rotation to crustal blocks in southern Oregon (see Figure 14 of MC07). In the east, rotation of the low-deforming Snake River Plain and the extending Great Basin may arise from differential extension across the Wasatch fault [*Payne et al*., 2012]. The Wasatch extension is likely driven by gravitational collapse of the elevated continent [*Jones et al*., 1996].

[44] Rotation may be enhanced by a strong pinning point. The rotation axes for the PNW blocks are close to being parallel, congregating in the region of the Idaho Batholith in central Idaho (Figure 5a). The Idaho Batholith is a major Cretaceous silicic magmatic intrusion in a relatively unextended region [*Gaschnig et al*., 2009] located west of the Centennial Tectonic Belt and north of the western Snake River Plain (Figure 1). The Idaho Batholith is underlain by a deep high-velocity seismic anomaly that may be thickened lithosphere, a deep crustal root or subducted Siletzia terrane [*Roth et al*., 2008; *Xue and Allen*, 2010; *Schmandt and Humphreys*, 2011; *Tian and Zhao*, 2012]. *Roth et al*. [2008] show the Idaho Batholith high-velocity root extending to ~300 km depth below the NE corner of Oregon and northern Idaho whereas *Schmandt and Humphreys* [2011] interpret separate velocity anomalies as depleted mantle and remains of the Siletzia slab. Such a thickened lithosphere or deep crustal root could cause excess drag on the lithosphere as it moves over the mantle.

[45] Similarly, *Wesnousky and Scholz* [1980] suggested that the craton of North America offers deep resistance to the westward motion of the plate over the mantle and modifies the crustal stress field, as evidenced by earthquake focal mechanisms. They show that east of the craton the crust is under contraction and extending to the west, and stress indicators show a circular pattern around the craton. A similar pattern is observed around the Idaho Batholith. GPS velocities from *Payne et al*. [2012, Figure 5] suggest that the region just west of the southern part of the Idaho Batholith is under contraction (though subtle) while to the east is the more obvious extension of the northern Basin and Range. If the Idaho Batholith is more strongly coupled to the mantle than surrounding regions, this pattern of deformation around it would indicate a westward flow of the mobile mantle relative to the crust/lithosphere. *Silver and Holt* [2002] argued for an eastward flow of the mantle relative to North America based on shear-wave splitting while *Liu and Bird* [2002] reached the opposite conclusion, that North America is driven west to some degree by a faster westward-moving mantle. In the latter case, the Idaho Batholith may be driven faster to the west than surrounding regions, leading to extension at its trailing (eastern) edge and compression to the west. Stress directions from a variety of sources reveal a ~90° change across the Idaho Batholith [see *Humphreys and Coblentz*, 2007, Figure 2a]. East of the Idaho Batholith, SHmax trends NW (NE-directed extension) whereas to the SW of the Idaho Batholith, SHmax is NE (NW-directed extension), suggesting that the Idaho Batholith has some fundamental influence on the local near-surface stress field [*Humphreys and Coblentz*, 2007].

[46] Although we lack sufficiently dense surface velocities or other constraints to determine its role, geodetic velocities in the southern part of the Idaho Batholith relative to those in northern Idaho suggest the batholith is not moving as a single uniform region [e.g., *Hamilton*, 1963]. The southern part of the Idaho Batholith may be moving west relative to the more stable northern part, consistent with a westward push by the mantle [*Payne et al*., 2012]. Such differential movement may be marked by a zone of seismicity that cuts through the Idaho Batholith [*Smith and Sbar*, 1974; *Smith and Lindh*, 1978; *Dewey*, 1987]. Three small to moderate size (magnitudes 4.9, 6.0, and 6.1) earthquakes have occurred in this zone suggesting some internal deformation within the Idaho Batholith [*Smith and Sbar*, 1974; *Dewey*, 1987].

4. Conclusions

[47] We have used a combination of horizontal and vertical geodetic data from the U.S. Pacific Northwest to examine the active tectonics and dynamics of the region. Models of locking on the Cascadia subduction zone based on vertical and horizontal geodetic data indicate that locking is broader beneath the central Oregon section than to the south. Rates of moment accumulation are consistent with great earthquakes every few hundred years. Geodetic rates of deformation across the Yakima fold-thrust belt in Washington reveal shortening in a fan-like fashion about a pole to the east, but are two orders of magnitude faster than the rates inferred from summed earthquake moments of the past half century. Geodetic moment rates are consistent with an *M*7 every couple of centuries. The rotation of eastern Oregon in a nearly rigid fashion above

a deforming mantle suggests either that they are decoupled or that the crust is stronger than the mantle. Although speculative, the coincidence of the rotation axes near the Idaho Batholith for many of the crustal blocks suggests that its deep, high-velocity root may play a role in modifying the stress field and deformation in the northwestern U.S.

[48] **Acknowledgments**. Much of the raw GPS data used in this work are from the UNAVCO (http://facility.unavco.org/data/data.html) and Northern California Earthquake Data Center (http://www.ncedc.org/survey-gps/) archives, deposited there by many researchers. Additional survey-mode GPS data were provided by the U.S. Geological Survey (USGS), Cascades Volcano Observatory (USGS), National Geodetic Survey, numerous county surveyors, Pacific Geoscience Centre, Base Mapping and Geomatic Services of British Columbia, Victoria Capital Regional District. Continuous data are courtesy of operators of the Plate Boundary Observatory, Pacific Northwest Geodetic Array, Western Canada Deformation Array, Bay Area Regional Deformation Array and National Geodetic Survey Continuously Operating Reference Stations sites. Scripps Orbit and Permanent Array Center provided global rinex files, precise orbits, and IGS solutions. Wayne Thatcher shared unpublished GPS data and thoughts. Ray Wells provided geologic guidance, Jeanne Hardebeck provided software and assistance and Fred Pollitz gave us results of his models. Figures were generated with the Generic Mapping Tool (Wessel and Smith, 1991). Supported by National Science Foundation grants EAR-0745624 and EAR-1062251 and National Earthquake Hazards Research Program grant 2010–0006.

References

Atwater, B. F. (1987), Evidence for great Holocene earthquakes along the outer coast of Washington state, *Science*, *236*, 942–944.

Atwater, T. (1970), Implications of plate tectonics for the Cenozoic evolution of western North America, *Geol. Soc. Am. Bull.*, *81*, 3513–3536.

Bakun, W. H., R. A. Haugerud, M. G. Hopper, and R. S. Ludwin (2002), The December 1872 Washington state earthquake, *Bull. Seismol. Soc. Am.*, *92*, 3239–3258.

Bird, P. (2009), Long–term fault slip rates, distributed deformation rates, and forecast of seismicity in the western United States from joint fitting of community geologic, geodetic, and stress direction data sets, *J. Geophys. Res.*, *114*, B11403, doi:10.1029/2009JB006317.

Blakely, R. J., B. L. Sherrod, C. S. Weaver, R. E. Wells, A. C. Rohay, E. A. Barnett, and N. E. Knepprath (2011), Connecting the Yakima fold and thrust belt to active faults in the Puget Lowland, Washington, *J. Geophys. Res.*, *116*, B07105, doi:10.1029/2010JB008091.

Burgette, R. J., R. J. Weldon, and D. A. Schmidt (2009), Interseismic uplift rates for western Oregon and along–strike variation in locking on the Cascadia subduction zone, *J. Geophys. Res.*, *114*, B01408, doi:10.1029/2008JB005679.

Campbell, N. D., and Bentley, R. D. (1981), Late Quaternary deformation of the Toppenish Ridge uplift in south–central Washington, *Geology 9*:519–524.

DeMets, C., R. G. Gordon, and D. F. Argus (2010), Geologically current plate motions, *Geophys. J. Int.*, doi:10.1111/j.1365–246X.2009.04491.x

Dewey, J. W. (1987), Instrumental seismicity of central Idaho, *Bull. Seismol. Soc. Am.*, *77*, 819–836.

Dragert, H., R. D. Hyndman, G. C. Rogers, and K. Wang (1994), Current deformation and the width of the seismogenic zone of the northern Cascadia subducted thrust, *J. Geophys. Res.*, *99*, 635–668.

Dragert, H., and R. D. Hyndman (1995), Continuous GPS monitoring of elastic strain in the northern Cascadia subduction zone, *Geophys. Res. Lett.*, *22*, 755–758.

Eagar, K. C., M. J. Fouch, D. E. James, and R. W. Carlson (2011), Crustal structure beneath the High Lava Plains of eastern Oregon and surrounding regions from receiver function analysis, *J. Geophys. Res. 116*, B02313, doi:10.1029/2010JB007795.

England, P., and R. E. Wells (1991), Neogene rotations and quasi–continuous deformation of the Pacific Northwest Continental Margin, *Geology*, *19*, [10], 978–981.

Flesch, L. M., W. E. Holt, A. J. Haines, L. Wen, and B. Shen–Tu (2007), The dynamics of western North America: Stress magnitudes and the relative role of gravitational potential energy, plate interaction at the boundary and basal tractions, *Geophys. J. Int. 169*, 866–896.

Fluck, P., R. D. Hyndman, and K. Wang (1997), Three–dimensional dislocation model for great earthquakes of the Cascadia subduction zone, *J. Geophys. Res.*, *102*, 20,539–20,550.

Fujiwara, T., S. Kodaira, T. No, Y. Kaiho, N. Takahashi, and Y. Kaneda (2011), The 2011 Tohoku–Oki Earthquake: Displacement Reaching the Trench Axis, *Science*, *334*(6060), 1240, doi:10.1126/science.1211554.

Gaschnig, R. M., J. D. Vervoort, R. S. Lewis, and W. C. McClelland (2009), Migrating magmatism in the northern US Cordillera: in situ U–Pb geochronology of the Idaho Batholith, *Contrib. Mineral. Petrol.*, doi:10.1007/s00410–009–0459–5.

Gilbert, H. (2012), Crustal structure and signatures of recent tectonism as influenced by ancient terranes in the western United States, *Geosphere*, *8*, 141–157, doi:10.1130/GES00720.1.

Goldfinger, C., C. H. Nelson, A. E. Morey, J. E. Johnson, J. Patton, E. Karabanov, J. Gutiérrez–Pastor, A. T. Eriksson, E. Gràcia, G. Dunhill, R. J. Enkin, A. Dallimore, and T. Vallier (2012), Turbidite event history—Methods and implications for Holocene paleoseismicity of the Cascadia subduction zone, U.S. Geological Survey Professional Paper 1661–F, 170 p, 64 figures, available at http://pubs.usgs.gov/pp/pp1661f/.

Gomberg, J., B. Sherrod, M. Trautman, E. Burns, and D. Snyder (2012), Contemporary seismicity in and around the Yakima Fold-and-Thrust Belt in eastern Washington, *Bull. Seismol. Soc. Amer.*, *102*, 309–320, doi:10.1785/0120110065.

Hamilton, W. (1963), Overlapping of Late Mesozoic orogens in western Idaho, *Geol. Soc. Am. Bull.*, *74*, 779–788.

Hammond, W. C., G. Blewitt, and C. Kreemer (2011), Block modeling of crustal deformation of the northern Walker Lane and Basin and Range from GPS velocities, *J. Geophys. Res.*, *116*, B04402, doi:10.1029/2010JB007817.

Hardebeck, J. L., and A. J. Michael (2006), Damped regional–scale stress inversions: Methodology and examples for southern California and the Coalinga aftershock sequence, *J. Geophys. Res.*, *111*, B11310, doi:10.1029/2005JB004144.

Herring, T. A. (2004), GLOBK: Global Kalman filter VLBI and GPS analysis program, Release 10.2, Mass. Instit. of Technol, Cambridge.

Herring, T., M. Craymer, G. Sella, R. Snay, G. Blewitt, D. Argus, Y. Bock, E. Calais, J. Davis, and M. Tamisiea (2008), SNARF 2.0: A regional reference frame for North America, *EOS Trans. Am. Geophys. Union*, *89*(Joint Assem. Suppl.), G21B–01.

Herring, T. A., R. W. King, and S. C. McCluskey (2010), Introduction to GAMIT/GLOBK, Release 10.4, Massachusetts Institute of Technology, Cambridge, Mass., 48 pp. (http://www–gpsg.mit.edu/~simon/gtgk/docs.htm).

Humphreys, E. D., and D. D. Coblentz (2007), North American dynamics and western U.S. tectonics, *Rev. Geophys.*, *45*, RG3001, doi:2005RG000181.

Hyndman, R. D., and K. Wang (1993), Thermal constraints on the zone of major thrust earthquake failure: The Cascadia subduction zone, *J. Geophys. Res.*, *98*, 2039–2060.

Jackson, J. (2002), Faulting, flow, and the strength of the continental lithosphere, *Int. Geol. Rev.*, *44*, 39–61.

Jones, C. H., J. R. Unruh, and L. J. Sonder (1996), The role of gravitational potential energy in active deformation in the southwestern US, *Nature*, *381*, 37–41.

Khazaradze, G., A. I. Qamar, and H. Dragert (1999), Tectonic deformation in western Washington from continuous GPS measurements, *Geophys. Res. Lett.*, *26*, 3153–3158.

Kostrov, B. V. (1974), Seismic moment and energy of earthquakes, and seismic flow of rocks, *IASUPSE*, *1*, 23–44.

Ladinsky, T. C., H. Kelsey, B. Sherrod, and T. Pratt (2010), Range–front deformation on the northern limb of the Manastash Anticline, Yakima Fold Belt, Washington (abstract), Eos AGU EP53B–0620.

Liu, Z., and P. Bird (2002), North America plate is driven westward by lower mantle flow, *Geophys. Res. Lett.*, *29*(24), 2164, doi:10.1029/2002GL016002.

Long, M. D., H. Gao, A. Klaus, L. S. Wagner, M. J. Fouch, D. E. James, and E. D. Humphreys (2009), Shear wave splitting and the pattern of mantle flow beneath eastern Oregon, *Earth Planet. Sci. Lett.*, *288*, 359–369, doi:10.1016/j.epsl.2009.09.039.

Ludwin, R. S., C. S. Weaver, and R. S. Crosson (1991), Seismicity of Washington and Oregon, in *Neotectonics of North America*, edited by D. B. Slemmons, E. R. Engdahl, M. D. Zoback, and D. D. Blackwell, pp. 77–97, Geological Society of America, Boulder, CO, US.

Magill, J., R. E. Wells, R. W. Simpson, and A. V. Cox (1982), Post 12 m.y. rotations of southwestern Washington, *J. Geophys. Res.*, *87*, 3761–3776.

McCaffrey, R. (1995), DEFNODE users' guide (http://sps.unavco.org/modeling/#defnode).

McCaffrey, R. (2002), Crustal block rotations and plate coupling, in Stein, S. and Freymueller, J., eds., *Plate Boundary Zones*, Am. Geophys. Union Geodynamics Series, vol. *30*, 101–122.

McCaffrey, R. (2005), Block kinematics of the Pacific – North America plate boundary in the southwestern US from inversion of GPS, seismological, and geologic data, *J. Geophys. Res.*, *110*, B07401, doi:10.1029/2004JB003307.

McCaffrey, R. (2009), Time–dependent inversion of three–component continuous GPS for steady and transient sources in northern Cascadia, *Geophys. Res. Lett.*, *36*, L07304, doi:10.1029/2008GL036784.

McCaffrey, R., A. I. Qamar, R. W. King, R. Wells, G. Khazaradze, C. A. Williams, C. W. Stevens, J. J. Vollick, and P. C. Zwick (2007), Fault locking, Block Rotation and Crustal Deformation in the Pacific Northwest, *Geophys. J. Int.*, *169*, 1315–1340, doi:10.1111/j.1365–246X.2007.03371.x.

McCaffrey, R., M. Long, C. Goldfinger, P. C. Zwick, J. L. Nabelek, C. K. Johnson, and C. Smith (2000), Rotation and plate locking at the southern Cascadia subduction zone, *Geophys. Res. Lett.*, *27*, 3117–3120.

McCrory, P. A., J. L. Blair, D. H. Oppenheimer, and S. R. Walter (2003), Depth to the Juan de Fuca slab beneath the Cascadia subduction margin: A 3–D model for sorting earthquakes, *U.S. Geological Survey Digital Data Series*, 1 CD–ROM.

McKenzie, D., and J. Jackson (1983), The relationship between strain rates, crustal thickening, paleomagnetism, finite strain, and fault movements within a deforming zone, *Earth Planet. Sci. Lett. 65*, 182–202.

Miller, M., H. Dragert, E. Endo, J. T. Freymueller, C. Goldfinger, H. M. Kelsey, E. D. Humphpreys, D. J. Johnson, R. McCaffrey, J. S. Oldow, A. Qamar, and C. M. Rubin (1998), Precise measurements help gauge Pacific Northwest's earthquake potential, *EOS 79*, 269–275.

Mitchell, C. E., P. Vincent, R. J. Weldon, and M. A. Richards (1994), Present day vertical deformation of the Cascadia margin, Pacific Northwest, United States, *J. Geophys. Res.*, *99*, 12,257–12,277.

Nelson, A. R., S. Y. Johnson, H. M. Kelsey, R. E. Wells, B. L. Sherrod, S. K. Pezzopane, L. Bradley, and R. D. Koehler III (2003), Late Holocene earthquakes on the Toe Jam Hill fault, Seattle fault zone, Bainbridge Island, Washington, *Geol. Soc. Amer. Bull.*, *115*, 1388–1403.

Okada, Y. (1992), Internal deformation due to shear and tensile faults in a half–space, *Bull. Seismol. Soc. Amer.*, *82*, 1018–1040.

Parsons, T., and W. Thatcher (2011), Diffuse Pacific–North American plate boundary: 1000 km of dextral shear inferred from modeling geodetic data, *Geology*, *39*, 943–946, doi:10.1130/G32176.1,

Payne, S. J., R. McCaffrey, and R. W. King (2008), Strain rates and contemporary deformation in the Snake River Plain and surrounding Basin and Range from GPS and seismicity, *Geology*, *36*, 647–650.

Payne, S. J., R. McCaffrey, R. W. King, and S. A. Kattenhorn (2012), A new interpretation of deformation rates in the Snake River Plain and adjacent Basin and Range regions based on GPS measurements, *Geophys. J. Int.*, *189*, 101–122, doi:10.1111/j.1365–246X.2012.05370.x.

Pollitz, F. F., P. McCrory, D. Wilson, J. Svarc, C. Puskas, and R. B. Smith (2010), Viscoelastic–cycle model of interseismic deformation in the northwestern United States, *Geophys. J. Int.*, *181*, 665–696.

Pratt, T. (2012), Large–scale splay faults on a strike–slip fault system: The Yakima Folds, Washington State, *Geochem. Geophys. Geosyst.*, *13*, Q11004, doi:10.1029/2012GC004405.

Puskas, C. M., and R. B. Smith (2009), Intraplate deformation and microplate tectonics of the Yellowstone Hotspot and surrounding western U. S. interior, *J. Geophys. Res.*, *114*, B04410, doi:10.1029/2008JB005940.

Raisz, E. (1945), The Olympic–Wallowa lineament, *Am. J. Sci.*, *243–A*, 479–485.

Reidel, S. P., N. D. Campbell, K. R. Fecht, and K. A. Lindsey (1994), Late Cenozoic structure and stratigraphy of south–central Washington, *WA Div. Geol. Earth Resour. Bull. 80*:159–180.

Reidel, S. P., K. R. Fecht, M. C. Hagood, and T. L. Tolan (1989), The geologic evolution of the central Columbia Plateau, *Geol. Soc. Am. Spec. Paper 239*, p. 247–264.

Reilinger, R., S. McClusky, P. Vernant, and 22 co–authors (2006), GPS constraints on continental deformation in the Africa–Arabia–Eurasia continental collision zone and implications for the dynamics of plate interactions, *J. Geophys. Res.*, *111*, B05411, doi:10.1029/2005JB004051.

Roth, J. B., M. J. Fouch, D. E. James, and R. W. Carlson (2008), Three–dimensional seismic velocity structure of the northwestern United States, *Geophys. Res. Lett. 35*, L15304, doi:10.1029/2008GL034669.

Savage, J. C., M. Lisowski, and W. H. Prescott (1991), Strain accumulation in western Washington, *J. Geophys. Res.*, *96*, 14,493–14,507.

Savage, J. C., W. Gan, and J. L. Svarc (2001), Strain accumulation and rotation in the eastern California shear zone, *J. Geophys. Res. 106*, 21,995–22,007.

Schmandt, B., and E. D. Humphreys (2011), Seismically imaged relict slab from the 55 Ma Siletzia accretion to the northwest United States, *Geology*, *39*, 175–178, doi:10.1130/G31558.1.

Shen, Z.–K., R. W. King, D. C. Agnew, M. Wang, T. A. Herring, D. Dong, and P. Fang (2011), A unified analysis of crustal motion in southern California 1970–2004: The SCEC Crustal Motion Map, *J. Geophys. Res.*, submitted.

Sheriff, S. D. (1984), Paleomagnetic evidence for spatially distributed post–Miocene rotation of western Washington and Oregon, *Tectonics*, *3*, 397–408.

Siebert, L., and T. Simkin (2002), Volcanoes of the World: an illustrated catalog of Holocene volcanoes and their eruptions. Smithsonian Institution, *Global Volcanism Program Digital Information Series*, **GVP–3**, (http://www.volcano.si.edu/world/).

Silver, P. G., and W. E. Holt (2002), The mantle flow field beneath western North America, *Science*, *295*, 1054–1057.

Simpson, R. W., and A. V. Cox (1977), Paleomagnetic evidence for tectonic rotation of the Oregon Coast Range, *Geology*, *5*, 585–598.

Smith R. B., and M. L. Sbar (1974), Contemporary tectonics and seismicity of the western United States with emphasis on the Intermountain seismic belt, *Geol. Soc. Am. Bull. 85*, 1205–1218.

Smith, R. B., and A. G. Lindh (1978), Seismicity, crustal structure, and intraplate tectonics of the interior of the western cordillera; in Smith, R. B. and Eaton, G. P., editors, *Cenozoic Tectonics and Regional Geophysics of the Western Cordillera*, Geological Society of America Memoir 152, 111–144.

Svarc, J. L., J. C. Savage, W. H. Prescott, and M. H. Murray (2002), Strain accumulation and rotation in western Oregon, and southwestern Washington, *J. Geophys. Res.*, *107*, 10.1029/2001JB000625.

Tian, Y., and D. Zhao (2012), P–wave tomography of the Western United States: Insight into the Yellowstone hotspot and the Juan de Fuca slab, *Phys. Earth Planet. Inter.*, doi:10.1016/j.pepi.2012.04.004.

Wang, K. (1996), Simplified analysis of horizontal stresses in a buttressed forearc sliver at an oblique subduction zone, *Geophys. Res. Lett.*, *23*, 2021–2024.

Wang, K., R. Wells, S. Mazzotti, R. D. Hyndman, and T. Sagiya (2003), A revised dislocation model of interseismic deformation of the Cascadia subduction zone, *J. Geophys. Res.*, *108*, 2026, doi:10.1029/2001JB001227.

Wells, R. E., and P. L. Heller (1988), The relative contribution of accretion, shear, and extension to Cenozoic tectonic rotation in the Pacific Northwest, *Geol. Soc. Amer. Bull.*, *100*, 325–389.

Wells, R. E., C. S. Weaver, and R. J. Blakely (1998), Fore arc migration in Cascadia and its neotectonic significance, *Geology*, *26*, 759–762.

Wernicke, B. P., A. M. Friedrich, N. A. Niemi, R. A. Bennett, and J. L. Davis (2000), Dynamics of plate boundary fault systems from Basin and Range Geodetic Network (BARGEN) and geologic data, *GSA Today*, *10*, 1–3.

Wesnousky, S., and C. Scholz (1980), The craton: Its effects on the distribution of seismicity and stress in North America, *Earth Planet. Sci. Lett.*, *48*, 348–355.

Wessel, P., and W. H. F. Smith (1991), Free software helps map and display data, *EOS Trans. AGU*, *72*, 441.

West, M. W., F. X. Ashland, A. J. Busacca, G. W. Berger, and M. E. Shaffer (1996), Late Quaternary deformation, Saddle Mountains anticline, south–central Washington, *Geology 24*:1123–1126.

Williams, C. A., and G. Wadge (1998), The effects of topography on magma chamber deformation models: Application to Mt. Etna and radar interferometry, *Geophys. Res. Lett. 25*, 1549–1552.

Williams, S. D. P. (2003), The effect of coloured noise on the uncertainties of rates estimated from geodetic time series, *J. Geod.*, *76*, 483–494.

Xue, M., and R. M. Allen (2006), Origin of the Newberry hotspot track: evidence from shear-wave spitting, *Earth Planet. Sci. Lett. 244*, 315–322.

Xue, M., and R. M. Allen (2010), Mantle structure beneath the western United States and its implications for convection processes, *J. Geophys. Res. 115*, B07303, doi:10.1029/2008JB006079.

Yeats, R. (2012), Active Faults of the World, Cambridge University Press.